In situ curing of liquid epoxy via gold-nanoparticle mediated photothermal heating

2017 Nanotechnology 28 065601

(http://iopscience.iop.org/0957-4484/28/6/065601)

IOP Publishing Nanotechnology
Nanotechnology 28 (2017) 065601 (9pp) doi:10.1088/1361-6528/aa521b

In situ curing of liquid epoxy via gold-nanoparticle mediated photothermal heating

Ju Dong[1,3], Gabriel E Firestone[2,3], J R Bochinski[2], L I Clarke[2,4] and R E Gorga[1,4]

[1] Fiber and Polymer Science Program, NC State University, Raleigh NC 27695, USA
[2] Department of Physics, NC State University, Raleigh NC 27695, USA

E-mail: liclarke@ncsu.edu and regorga@ncsu.edu

Received 24 August 2016, revised 25 November 2016
Accepted for publication 6 December 2016
Published 3 January 2017

Abstract

Metal nanoparticles incorporated at low concentration into epoxy systems enable *in situ* curing via photothermal heating. In the process of nanoparticle-mediated photothermal heating, light interacts specifically with particles embedded within a liquid or solid material and this energy is transformed into heat, resulting in significant temperature increase local to each particle with minimal warming of surroundings. The ability to use such internal heating to transform the mechanical properties of a material (e.g., from liquid to rigid solid) without application of damaging heat to the surrounding environment represents a powerful tool for a variety of scientific applications, particularly within the biomedical sector. Uniform particle dispersion is achieved by placing the nanoparticles within solvent miscible with the desired epoxy resin, demonstrating a strategy utilizable for a wide range of materials without requiring chemical modification of the particles or epoxy. Mechanical and thermal properties (storage modulus, T_g, and degradation behavior) of the cured epoxy are equivalent to those obtained under traditional heating methods. Selective curing of a shape is demonstrated within a liquid bath of epoxy, where the solid form is generated by rastering a spatially confined, photothermal-driving light beam. The non-irradiated regions are largely unaffected and the solid part is easily removed from the remaining liquid. Temperature profiles showing minimal heating outside the irradiated zone are presented and discussed.

Keywords: thermoset, metal nanoparticles, photothermal heating, *in situ* curing, laser rastering

(Some figures may appear in colour only in the online journal)

1. Introduction

The ability to transform the mechanical properties of a material *in situ* would be a powerful tool for biomedical applications. For example, one can envision a soft, flexible object that can be compressed (e.g., folded or rolled) and inserted within the body requiring a minimal incision size before subsequently being expanded and rigidified to serve a functional purpose. Not only is a mechanically soft material capable of forming a compact configuration, such a flexible object is less likely to damage surrounding tissue when being implanted and positioned. For instance, a soft polymer fiber or nanofibrous web filled with liquid epoxy resin could be placed within a bone break without damage to the surrounding, intact tissue, and then cross-linked *in situ* to provide a tissue scaffold with suitable rigidity and stiffness to stimulate bone growth. The final mechanical properties of tissue scaffolds are particularly important because local stem cells that migrate to a wound within any tissue are influenced by a variety of environmental factors (including stiffness) that determine the differentiation pathway along which the stem cells progress (i.e., local environment determines the type of tissue (e.g., bone, connective, fat) that ultimately results from the stem cells) [1–5]. Materials with dramatically controllable moduli could contribute to a new 'healing from within' paradigm in biomedical applications where indigenous proteins or stem cells within the body are recruited to migrate to a

[3] These authors contributed equally to this work.
[4] Authors to whom any correspondence should be addressed.

material device by suitable choice of materials. This transformative approach within medicine (e.g., already in use for artificial joints [6]) results in healing and repair passively stimulated by material design.

Thermosets (such as epoxy) are polymeric materials which undergo dramatic changes in mechanical properties (occurring generally by transforming from an unconstrained liquid to a rigid, tough solid) when heated, which drives a cross-linking reaction between the resin chains. Thermosets cross-link at temperatures in the 50–100 °C range—levels which would cause significant damage to surrounding biological tissues if curing took place within a living being via conventional means. However, if heat could be selectively generated only in the interior of the thermoset material, then the temperatures on the object's surface would remain significantly lower. In the selective process of plasmon-mediated photothermal heating, light interacts specifically with embedded nanoparticles and is transformed into heat locally, resulting in significant temperature increase near each nanoparticle with minimal warming of the surroundings [7–10, 25, 33–35]. Previous work has shown that even objects in physical contact with photothermally heated material may have a negligible increase in temperature [7]. This process relies on the localized surface plasmon resonance (SPR) of metal nanoparticles, which can be tuned significantly by altering particle composition, shape, and size [11–13]. Thus, the light intensities and wavelengths required for photothermal heating can be adjusted to ensure minimal effect on the surrounding material: for instance, with anisotropic nanoparticles the SPR can easily be tuned within the first so-called near-infrared window (∼650–950 nm for biological tissues [14]) where interaction with tissue is minimized [15, 16].

In this report, a proof-of-principle study demonstrates that photothermal heating can be usefully utilized to cross-link epoxy with minimal heating of the surroundings—a fundamental capability that would enable the applications discussed above. In order to test the selectivity of heating and the temperature rise in non-irradiated regions, lines of a thermoset are cross-linked within an epoxy bath by controllably scanning a collimated laser beam in the desired pattern within the liquid, then removing unaffected epoxy, leaving the resultant cross-linked object. This configuration (forming a shape via cross-linking of an unconfined liquid precursor) also has implications for three-dimensional printing without need for lamination, which is an approach likely to produce enhanced mechanical properties in comparison with the traditional layer-by-layer scheme [17]. Epoxy matrix with hardener (i.e., cross-linking agent) can present a corrosive environment for metal, thus strategies to efficiently incorporate metallic nanoparticles were developed. The mechanical properties of thermoset cross-linked via photothermal heating are shown to be identical to those measured in samples cured by conventional means. Temperature profiles from the irradiated region outward are discussed. In all cases, a spatially scanning laser beam is utilized so that in the future arbitrary shapes can be generated.

2. Experimental

2.1. Gold nanoparticle fabrication

Metal nanoparticles are utilized in a plethora of diverse technical applications, including for subwavelength confinement in nano-photonic devices [18], to generate enhanced scattering in biological imaging [19, 20], or as nanoscale electronic components in fundamental charge transport studies [21–24]. In recent years, their photothermal effect [25, 26] (e.g., the ability to efficiently convert optical energy into local heat) has been frequently exploited. Spherical gold nanoparticles (AuNP) were synthesized using the Frens method [27]. A near boiling aqueous solution of tetrachloroauric(III) acid (Sigma-Aldrich) was reduced with sodium citrate (Sigma-Aldrich) to form well-dispersed, citrate-stabilized gold nanospheres. Upon cooling, powdered polyvinylpyrrolidone (PVP) (360 kg mol^{-1}, Scientific Polymer Products, Inc.), in an amount equal to the original mass of tetrachloroauric acid was added to further stabilize the nanoparticles, including for solvent exchange. The AuNP were characterized in two ways. AuNP solution was drop-cast on copper grids for inspection via transmission electron microscopy (TEM) (JEM 2000FX), which revealed roughly spherical particles with diameter 19 ± 7 nm ($n = 75$). In addition, ultraviolet-visible (UV–vis) absorption spectroscopy (Cary 50 Scan) showed a SPR peaked at 521 nm, indicating a particle diameter of 18–20 nm, and a peak amplitude yielding an estimated concentration of 1.3–1.6 nM [28]. These values are consistent with TEM results for size and with the expectation for concentration assuming almost complete conversion of the gold salt to gold within the nanoparticles.

To facilitate solvent exchange, PVP-stabilized aqueous AuNP solutions were first dehydrated to 1/30th of original volume by placing them in conventional oven at 60–65 °C for 4–5 d. Solvent exchange involved incrementally adding dimethylformamide (DMF) (Sigma-Aldrich) to the concentrated solution within the oven as additional water evaporated until the majority of the water had been removed (an additional 2–3 d, 60–65 °C). Final concentration of the AuNP in DMF as measured from UV–vis observations was 29 nM indicating minor losses, with a SPR peak shift to 532 nm, as expected due to the change in dielectric constant of the solvents [29].

2.2. Epoxy systems

Two epoxy systems were utilized in this work. System 1 consisted of epoxy resin polyglycol di-epoxide (DER 736, Olin Epoxy) and triethylenetetramine curing agent (DEH 24, DOW Epoxy). System 2 consisted of resin bisphenol-A-diglycidyl ether (20-3302RCL, Epoxies, etc) and polyoxypropylenediamine based curing agent (20-3302CCL, Epoxies, etc). Both systems exhibit relatively low viscosity and long pot life in uncured form. Epoxy system 2 is more rigid than system 1 after curing and is optically clear from 400–600 nm which aids the perylene fluorescence measurement (see section 2.4). System 1 (2) consisted of a 9:1 (5:3)

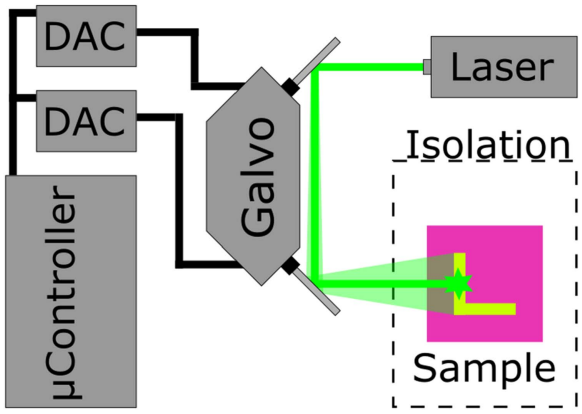

Figure 1. Schematic of laser rastering system. 'Galvo' refers to the 2-axis mirror galvanometer system (SpaceLas). 'DAC' are the MCP4725 digital-to-analog converter breakouts, controlled by any microcontroller with I2C output (Raspberry Pi). The sample is a glass coverslip supporting a thin layer of epoxy liquid. The green (532 nm) laser is deflected by the mirrors to trace out an arbitrary pattern (L shape in the schematic). The sample is surrounded by an aluminum cover with an access opening through which the laser passes.

epoxy:hardener ratio by volume and cured at 60–65 °C (52–55 °C) for 2 (2) hours, respectively. Both systems cross-link via the same reaction: briefly, the amine nitrogen atom attacks the epoxy ring at its terminal carbon; a primary amine can react in this way with two epoxy groups, such as in epoxy system 2, while a secondary amine can react with only one epoxy group as in epoxy system 1.

2.3. Apparatus

For conventional heating experiments, samples were cured using a commercial hotplate (VWR 7 × 7 CER) upon which was placed a 40 × 70 × 9 mm copper block having an embedded type T thermocouple (Omega Engineering). A customized aluminum cover was placed over the hotplate to provide isolation from ambient air currents without blocking the optical path needed for later photothermal curing. Epoxy liquid was poured onto clean glass coverslips (VWR) on the unheated copper block, which was then raised to the curing temperature as monitored by a second thermocouple immersed in the liquid, and allowed to cure for the designated time.

One challenge in utilizing photothermal heating for fabrication of macroscopic objects is the need to irradiate a large spatial region, which for continuous illumination may require expensive, high power laser systems to obtain sufficient light intensity across the entire shape. In the research presented here, an alternative approach of rapidly and controllably moving a small, focused light spot over a much larger area (figure 1) is employed, which is referred to as laser 'rastering'. In particular, a 532 nm, 4 W continuous-wave diode laser manipulated with converging lenses formed an approximately collimated, $1/e^2$ spot diameter of 1.9 mm. Using a 2-axis mirror galvanometer system (SpaceLas PT-20K) controlled by dual MCP4725 12-bit digital-to-analog converters (Adafruit Industries), the laser spot was scanned across a horizontal sample surface mounted on a copper block, where access to the sample was through a hole in the aluminum cover. The laser beam power was manually adjusted over the range 0.3–0.8 W by rotating the linear polarization direction with a $\lambda/2$ waveplate (Melles Griot) relative to a fixed Glan–Thompson polarizer (Thorlabs), then subsequently making the beam circularly polarized with a $\lambda/4$ waveplate (Melles Griot).

It can be shown by explicitly monitoring the average sample temperature (see section 2.4) in the irradiated and nearby non-irradiated regions for a wide range of laser intensities, with and without laser rastering, and by iterating the pattern at different scan rates, that if the laser spot returns to each spatial point on the pattern within a time period which is short compared to the time required for the heat to transport away from the irradiated area, all rastering rates result in identical heating outcomes. Under continuous (i.e. non-scanning) photothermal heating, the important parameter is the laser spot intensity (laser power/cross-sectional area of the laser beam). When rastering, the time-averaged intensity (laser power/cross-sectional area of the illuminated pattern) is the controlled and pertinent quantity. The raster rate refers to the frequency with which the scanning pattern is repeated; for all raster rates over the same pattern using the same laser power, the time-averaged intensity is the same. We observe that when irradiating sample regions centimeters in size, applying raster rates greater than 1 Hz results in essentially equivalent temperature changes for polymeric materials (including epoxy) because thermal transport within polymers is a relatively slow process [30], occurring on the order of minutes. For the experiments described in this work, triangle waves of 25 and 307 Hz (non-integer multiple frequencies) were used to drive the galvanometric mirrors that deflected the laser beam and thus traced out a two-dimensional shape within the thin layer (∼2 mm thick) of liquid epoxy (figure 1).

2.4. Internal temperature measurement

Perylene, a fluorescent dye molecule, was incorporated at a low concentration (0.005 weight percent (wt%)) in the uncured epoxy to enable an estimate of the average internal temperature during conventional and photothermal curing. Such an internal molecular thermometer enables confirmation of bulk temperature measurements (e.g., embedded thermocouples), which is particularly important for photothermal heating where the steady-state temperature within the sample is not homogeneous (with the region near each nanoparticle much warmer than the portions of the sample between nanoparticles) and internal and surface temperatures differ significantly. The thin films and liquid baths utilized in this work were less than 2 mm thick and thus difficult to monitor with external probes. Perylene molecules are distributed throughout the sample: thus the vast majority of the dye molecules are far from a nanoparticle [8]. The temperature near photothermally heated nanoparticles decreases rapidly over the first 100–200 nm, moving radially outward from the AuNP [8]. For the particle loading utilized in this work, the average AuNP particle–particle spacing is ∼1 μm, which

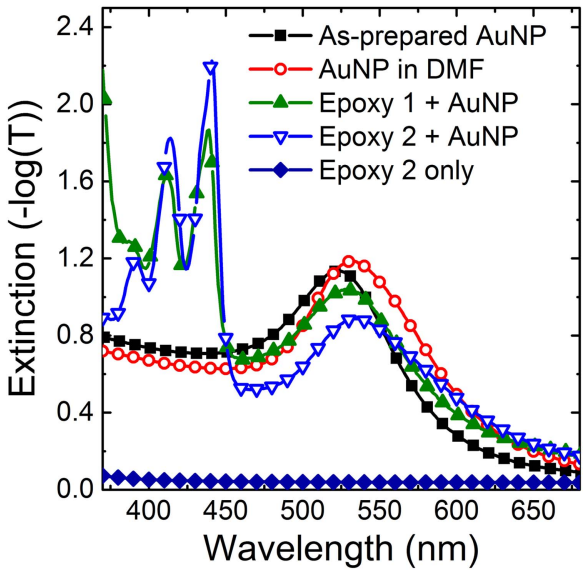

Figure 2. UV-vis absorption spectroscopy of the as-prepared aqueous AuNP solution (closed squares) reveals the distinctive SPR at ~520 nm. The ~30× concentrated AuNP solution in DMF (re-diluted in DMF to ~1×, open circles) shows an SPR shift to ~530 nm due to refractive index change of the solvent and no significant peak widening, indicating that the particles are still dispersed and intact. The same SPR position and breadth is present for the cured epoxy+AuNP 1 (closed triangles) and 2 (open triangle) films (which also contain perylene, generating the features at 400–450 nm).

means the maximum possible, average distance between a perylene molecule and a particle is 500 nm. 75% of the molecules reside in regions 300–500 nm from any particle and only about 5% of the perylene are within 180 nm of a particle, that is, within the region of significant sharp temperature increase. Thus, when monitoring the temperature increase due to photothermal heating, the perylene measurement most closely reflects the background temperature far from any nanoparticles. This is an appropriate comparison to the uniform sample temperature achieved via conventional heating.

When excited by 405 nm light, perylene fluoresces in the spectral range 430–530 nm (figure 2) with a characteristic emission shape which is sensitive to the local temperature of the surrounding material, as described previously [7–9, 30, 31]. Taking the ratio of the fluorescence amplitude at two different wavelengths (465 nm, which is a local minimum in the spectrum, over 475 nm, near a peak position) results in a ratio which is quasi-linear in temperature, and also robust to variation in illumination intensity or potential photo-bleaching. A violet, continuous-wave diode laser (MaXYZmodules 405 nm, 25 mW) was spatially filtered with a 50 μm pinhole, collimated into ~1 mm diameter beam having ~10 μW power and flywheel-chopped at 2 kHz. Laser fluctuations were separately monitored. The perylene fluorescence was imaged onto a double-grating scanning monochromator (SPEX 1680B) and the output signal was measured with a side-on photomultiplier tube (PMT) detector (Hamamatsu 931B). Optical filters blocked any unintentional scatter from either the violet (435 nm dielectric low-pass interference filter (Omega Optical)) or the green (532 nm, notch filter (CVI)) lasers. The amplified PMT output was photon-counted (Stanford Research Systems SR400) for both the active (with fluorescence present, violet laser on) and background measurements (with the violet laser blocked).

The 'peak-to-trough' fluorescence ratio is approximately linear with temperature having a slope and offset that depend on the modes of the local environment, which in this case, may change significantly during the curing process. Thus, actively monitoring the ratio during a curing process may convolve changes due to the increasingly stiff environment (switching between different ratio versus temperature 'lines') with changes due to temperature (moving along a single line). To obtain consistent results, measurements on fully cured films were utilized to establish the laser intensity required to match the average temperature during photothermal heating with that in conventional heating experiments. In particular, a calibration curve (converting perylene fluorescence ratio to temperature) was established by conventional heating a fully cured epoxy+AuNP film over the temperature range of 20–90 °C. The ratio was then monitored as fully cured films were photothermally heated in order to determine the requisite laser intensity to achieve an average temperature of 60–65 °C (52–55 °C) within epoxy+AuNP 1(2), respectively. These irradiation conditions were subsequently applied to uncured epoxy+AuNP liquid samples to cause cross-linking. Temperature values within the thermoset during curing were estimated by monitoring the perylene ratio and converting to estimated temperature by using the offset value at room temperature after curing and an estimated slope from the measurements on cured samples.

2.5. Sample characterization

The mechanical properties of cured epoxy and epoxy+AuNP were investigated using dynamic mechanical analysis (DMA) (Thermal Analysis Q800) in tension film mode from −60 °C to 100 °C with a heating rate of 3 °C min^{-1} (gauge length 10–12 mm). All measurements were carried out at 1 Hz with amplitude 15 μm and preload force of 0.01 N. Samples were cut from drop-cast films to approximately 6 × 15 × 0.8 mm. Decomposition was investigated using thermogravimetric analysis (TGA) (Perkin Elmer Pyris 1) under a nitrogen atmosphere. Sample masses of approximately 7 mg were heated from 30 °C to 600 °C at a rate of 20 °C min^{-1}. Extinction spectra of the AuNP, perylene, and epoxy were obtained from UV–vis spectrometry from 300 to 1100 nm wavelength with an integration time of 0.0125 s, using liquid samples in polycarbonate cuvettes having 1 cm path length and solid samples (epoxy +AuNP films) mounted in a homemade holder.

3. Results and discussion

3.1. Incorporation of AuNP into epoxy systems

One outcome of this work was to identify facile pathways to incorporate metallic nanoparticles, or other nanoscopic

objects that could be utilized for heating-from-within, into reactive materials. A challenge in this regard is degradation of particle quality or particle aggregation due to interaction with reactive species, such as curing or cross-linking agents. Additionally, nanoparticles (particularly, gold particles) are commonly fabricated in aqueous solution, which is incompatible with many polymeric systems including most thermosets. As described in the experimental section, AuNP solutions were concentrated and placed into a solution of DMF. Spectroscopy measurements indicated no significant aggregation, destabilization, or change in particle size due to the concentrating process (figure 2). DMF is miscible with the both epoxy matrices and thus provides a mechanism for particle incorporation.

For epoxy 1, optimal particle dispersion was obtained (figure 2) from a multi-step approach. First, epoxy resin and curing agent were combined and reacted slowly for 8–10 h at room temperature. This initial step minimized the attack of AuNP by the cross-linking agent. Then, this viscous liquid was combined with the nanoparticle/perylene/DMF solution. Immediately after initial mixing (i.e., before any evaporation of DMF), the liquid had an approximate composition by weight of ~80% epoxy, ~20% DMF, 0.01% AuNP, and 0.005% perylene, which will subsequently be referred to as epoxy+AuNP liquid 1. The viscosity of resultant liquid is appropriate for electrospinning in a core-sheath configuration with a liquid epoxy core. In general, this liquid (in a bath or within nanofibers) was then cross-linked by exposure to elevated temperature (e.g., 65 °C for 2 h). A similar, but single stage, approach was utilized for epoxy 2. Epoxy resin 2 was combined with cross-linking agent and then immediately mixed with the AuNP/perylene/DMF solution resulting in epoxy+AuNP liquid 2 having an approximate composition by weight of ~90% epoxy, ~10% DMF, 0.01% AuNP, and 0.005% perylene.

This scheme has multiple advantages. Solvent exchange enables particles fabricated in aqueous environment to be incorporated within organic solvent systems. This approach is straightforward due to the relatively high stability of the PVP-coated AuNP. The solution is concentrated by heating the solution in a narrow-necked vessel at moderate temperature (e.g., 60–65 °C for 2–3 d in a conventional oven) before another solvent with a higher boiling point (T_{bp}) is introduced. The higher boiling point solvent (for DMF, $T_{bp} = 153$ °C) has a lower vapor pressure than water, which continues to slowly vaporize at the moderate temperature over an additional 2–3 d. DMF is a polar aprotic solvent which ensures solubility and miscibility with a wide range of materials, including most epoxies. Thus, this method provides an alternative approach for high dispersion of gold nanoparticles within an epoxy matrix without requiring functionalization of the nanoparticle shell (i.e., the ligand matrix that commonly surrounds each particle) [32].

The AuNP/DMF solution was cooled in ambient to room temperature and then mixed with epoxy with cross-linking agent present, resulting in a slightly swollen epoxy matrix (10–20% DMF) with well-dispersed AuNP. The resultant epoxy+AuNP liquid can be cured immediately with DMF evaporation coincident with cross-linking. The thin film configuration utilized here has high surface area to volume which enhances DMF loss. In this approach the epoxy +AuNP liquid viscosity can be tuned over a wide-range to be suitable for various processing techniques. For example, if desired (e.g., for a nanofiber forming process such as electrospinning), pre-curing the epoxy before introducing AuNP/DMF increases viscosity without significant cross-linking. Conversely, swelling with DMF reduces the epoxy+AuNP liquid viscosity which can be controlled via the DMF: epoxy ratio.

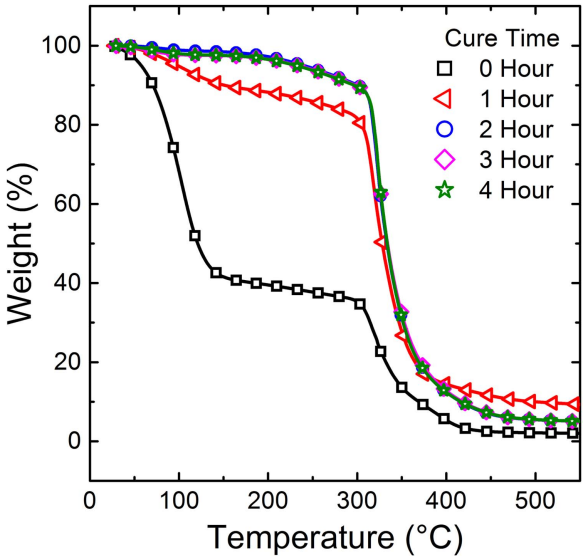

Figure 3. TGA scans of epoxy system 1 as a function of curing time at 65 °C. Complete sample curing is achieved after 2 h. In addition, the residual DMF present in the uncured and 1 h cured samples (i.e., the mass loss at ~160 °C) is minimized after 2 h processing time.

3.2. Optimal curing conditions

In order to determine optimal processing conditions, thin film samples (~1 mm thick) of epoxy+AuNP liquid 1 were conventionally cured at 65 °C for different time intervals. TGA showed no difference in the thermal stability of the network for curing times of 2 h or longer (figure 3). For lower cure times, the weight loss below 160 °C in the 0 and 1 h cured samples can be attributed to residual DMF evaporation. After the 2 h cure, no significant DMF is present. Epoxy degradation occurs at ~300 °C, which shifts from 304 ± 2 °C for a 0 h cure to 306 ± 2 °C (1 h), 312 ± 2 °C (2 h), 314 ± 2 °C (3 h), and 314 ± 2 °C (4 h), indicating that samples cured for 2 h or more are similar. Thus, for all further experiments, epoxy+AuNP liquid 1 was cured at 65 °C for 2 h. For epoxy +AuNP liquid 2, samples were cured according to the manufacturer's suggested protocol of 2 h at 52 °C.

3.3. Comparison between photothermal and conventional curing of epoxy

Green light at 532 nm is resonant with the SPR of the AuNP (figure 2) while epoxy has minimal absorption at this

wavelength. Thus, the optical energy from the applied laser beam will be virtually solely absorbed by the AuNP and then rapidly converted into heat (within ~100 ps [13]). This process causes each gold nanoparticle to serve as a nanometer-sized heater embedded within the liquid epoxy and enables curing from within. The temperature within the irradiated regions of the epoxy is inhomogeneous at the mesoscale, with warmer temperatures near each particle and cooler regions in the material further removed from any nanoparticles [8]. Nanoparticles are, on average, separated from their nearest neighbor by a distance of ~1 μm at the loading level employed. As discussed in section 2.4, the internal temperature measurement utilizing embedded perylene was employed to best match the overall average sample temperature achieved during heterogeneous photothermal heating with the mostly homogeneous temperature achieved under conventional treatment.

As a first experiment, tuned to match optimal conventional curing conditions, photothermally heated samples were cured at an average temperature of 65 °C for 2 h or 52 °C for 2 h, for epoxy+AuNP liquid 1 or 2, respectively. In particular, for photothermal treatment, the 532 nm wavelength laser spot of 1.90 mm diameter with a spot intensity of 23 W cm^{-2} was scanned over a rectangular area of 6 × 22 mm, which resulted in a time-averaged intensity of 0.48 W cm^{-2}. The laser beam traced out a two-dimensional shape within a thin film (~1.5 mm thick) bath of epoxy (figure 1), the sample was removed from the surrounding uncross-linked liquid material, and subjected to mechanical testing. Characteristic estimated temperature versus time curves for photothermal and conventional treatment of epoxy+AuNP liquid 1 (figure 4) indicate that the intentional match of the temperature versus time and the resultant epoxy curing processes are nearly identical. This enables a fair comparison between the photothermally and conventionally cured samples. Note that in the absence of nanoparticles neither evidence of curing nor any temperature increase (figure 4)[5] was observed when epoxy 1 liquid (with DMF and perylene but no AuNP) was exposed to identical irradiation.

Figure 5 shows representative mechanical properties of the photothermally cured epoxy-nanocomposite 1 in comparison with a conventionally cured sample. The average maximum storage moduli are 1.5 and 1.9 GPa, respectively, and the estimated glass transition temperature, (T_g) as indicated by the peak in tan δ, occurs at −11 °C or −13 °C. The differences in these values are within sample-to-sample variation. This observation suggests that photothermal heating produces a cross-linked network with mechanical properties essentially identical to those generated from curing with conventional means. Thus, the ability to cure completely via photothermal heating from a dilute concentration of nanoparticles is confirmed. Unlike conventional means, photothermal heating enables *in situ* curing without significant warming of the surroundings, as discussed in the next section.

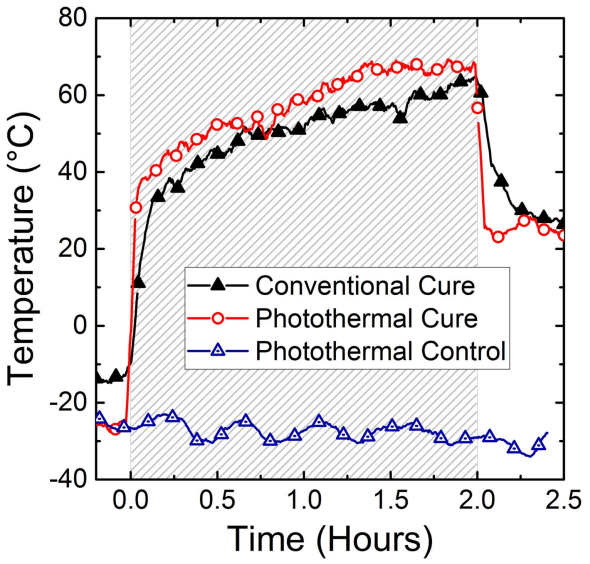

Figure 4. Estimated temperature versus time for conventional (filled triangles) and photothermal (open circles) curing of epoxy+AuNP liquid 1, demonstrating the ability to match the temperature profile and curing process. Heating is applied during the shaded region time interval. The sharp slope at short times results from a true temperature increase whereas the slower growth over longer times reveals changes in the mechanical properties due to curing. (See footnote 5.) As shown, photothermal heating under these conditions (1.9 mm diameter, 26 W cm^{-2} 532 nm laser rastered at 25 Hz) provides as rapid an increase in temperature as conventional heating and thus curing could in principle occur at short time scales with high efficiency. Here a two hour cure time is utilized to match the conventional results. Epoxy without AuNPs displayed no evidence of curing (open triangles).

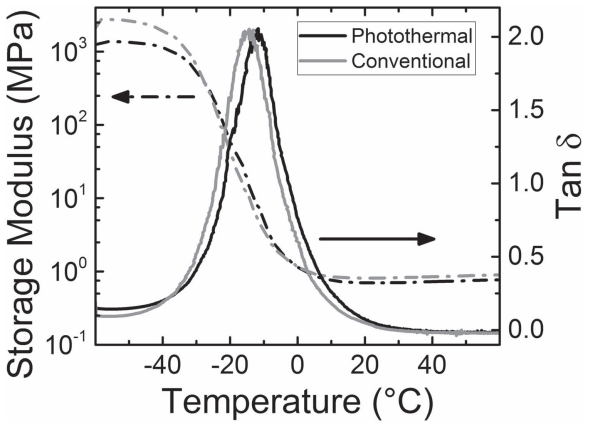

Figure 5. Comparison of the storage modulus and loss (tan (δ)) measured by DMA of film samples (epoxy+AuNP 1) cured at the same average temperature for the same time via either photothermal or conventional heating. The similar results indicate that both the mechanical properties and T_g are indifferent to the method of curing.

[5] The artificially low temperature values at short times are a result of using the calibration curve for a cured sample to convert observed ratio to temperature. This is appropriate at the end of curing however the system is softer at the beginning of the cross-linking process, resulting in a different conversion between temperature and observed ratio (a larger change in ratio with temperature). Thus temperature changes are artificially enhanced for times less than 1 h. An uncured sample cannot be calibrated because it would cure during the calibration process (see section 2.4).

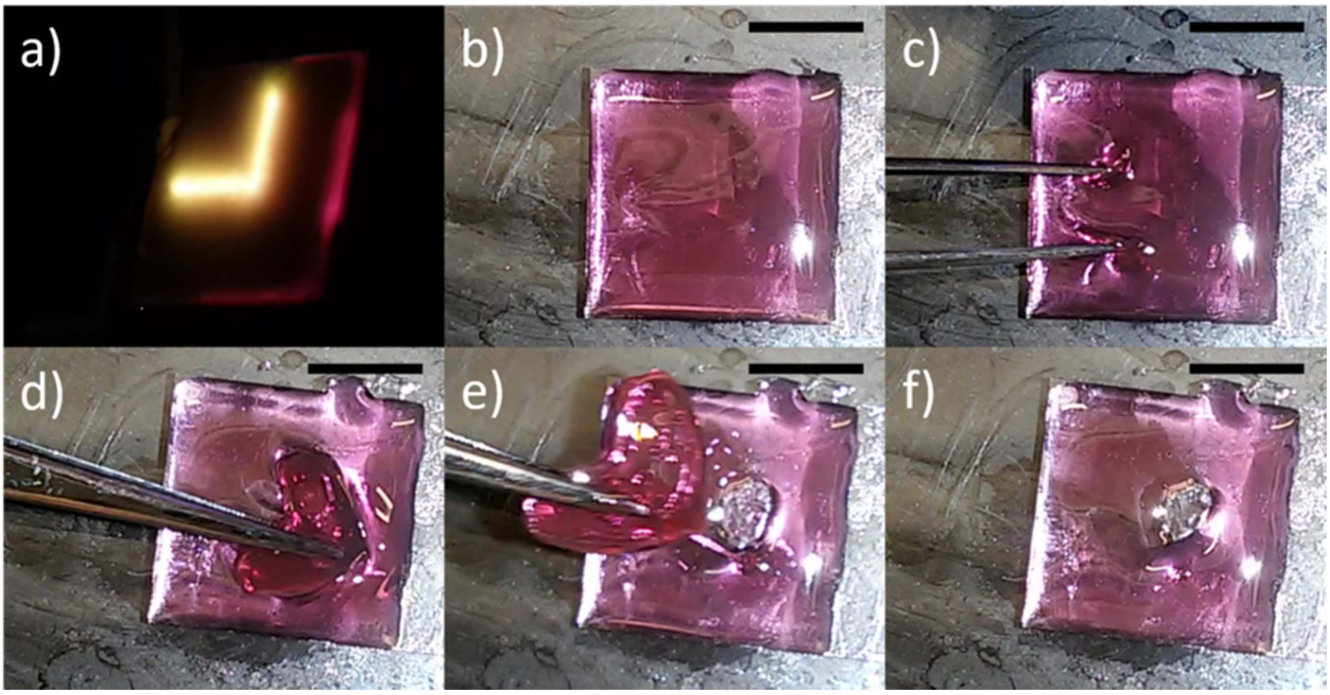

Figure 6. A characteristic selective *in-situ* curing experiment. (a) Pattern delineated by the rastering laser applied to the liquid epoxy. The edge of the epoxy+AuNP liquid-coated coverslip can be seen as faint pink lines. (b) The sample after curing of the selected region is complete. The cross-linked and liquid material cannot be distinguished by eye. (c)–(e) The formed shape is removed from the liquid. (f) Uncured liquid flows into the void space where the solid sample has been removed. The scale bar (same in all images and measured in the plane of the glass slide) is 1 cm.

3.4. Selective photothermal curing

A major benefit of photothermal heating is the ability to heat selected regions while leaving surroundings unaffected, the key characteristic that would enable thermal cross-linking of materials *in situ* within delicate environments. In this section, selective curing of a single region within an epoxy liquid bath, while the surrounding material remains liquid, is demonstrated. We quantify the temperature profile from the irradiated region outward; that is, the inadvertent heating of the immediate surroundings due to transfer from the heated zone. Figure 6 consists of a series of images demonstrating selective curing. First, epoxy+AuNP liquid 1 is placed on a glass coverslip, resulting in a liquid thin film bath ∼1.5 mm thick. To achieve the temperatures established above (see sections 3.2 and 3.3) for optimal curing, a 1.9 mm diameter 532 nm laser beam (with a spot intensity of 26 W cm^{-2} and time-averaged intensity of 2.0 W cm^{-2}) was rastered along an 'L shape' with ∼1 cm leg lengths having a line width defined by the beam diameter (figure 6(a)). After 2 h of laser irradiation, the cross-linked and liquid material were indistinguishable to the eye (figure 6(b)). However, by sweeping forceps through the bath, the solid region could be removed (figures 6(c)–(e)). The remaining uncross-linked material was still liquid and re-filled the void where the cured sample was removed (figure 6(f)).

The width of the straight regions of the cured part in figure 6 was approximately 5 mm, indicating that the temperature outside the irradiated region (itself ∼2 mm wide) dropped significantly in the 1.5 mm on each side. Beyond this 1.5 mm region, the temperature in the liquid was sufficiently low that no curing resulted. We note that this proof-of-principle experiment was not optimized toward producing particular shapes or object features but simply used to demonstrate the underlying concept.

In order to further estimate the temperature within the liquid bath during irradiation, the laser was rastered along a single straight line on a fully cured sample and the temperature as a function of distance from the center of the line was measured resulting in a cross-sectional temperature profile. Figure 7(a) presents such a temperature profile from a cured epoxy+AuNP 2 sample. The maximum observed temperature is 55 °C (34 °C above laboratory ambient temperature) and occurs at the center of the irradiated zone. The edge of the illuminated region is slightly cooler (∼50 °C). Regions of the sample far from the laser beam are only warmed by ∼5 °C, even after photothermal heating for several hours. The full-width-half-maximum (FWHM) of the temperature peak associated with the actively heated region is 3.9 mm, which indicates that the temperature drops dramatically in the 1.0 mm outside the irradiated region. As shown in figure 7(b), when these conditions are applied to cure epoxy+AuNP 2 liquid, the physical width of the resulting cross-linked epoxy sample ranges from 1.6 mm at the epoxy glass surface to 4.4 mm at the air epoxy surface where the laser is incident. All material further than 1.2 mm from the edge of the irradiated zone remained liquid and was removed after the curing process. These values are quantitatively consistent with the

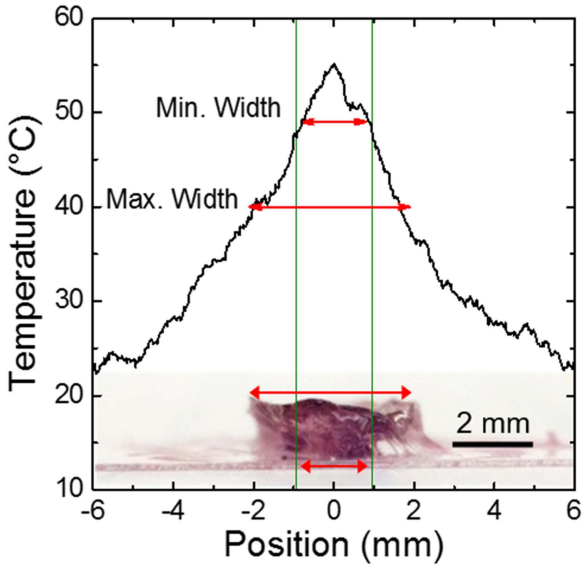

Figure 7. Temperature profile within a fully cured sample of epoxy +AuNP 2. The vertical green lines denote the $1/e^2$ diameter of the irradiated region. Inset: a cross-section of a line of epoxy+AuNP 2 cured under these conditions (line length 20 mm, spot intensity 13 W cm^{-2}, time-averaged intensity 1.0 W cm^{-2}, laser incident from above). As can be observed from the image, material was only cross-linked in the immediate vicinity of the laser driven heating. The scale of the image is matched to that of the temperature profile upon which the minimum and maximum observed cured epoxy widths are also indicated. The minimum width of the cross-linked line (1.6 mm) is similar to the laser width and its maximum (4.4 mm) is similar to the FWHM of the temperature profile. As discussed in the text, the observed curing width is completely consistent with the measured temperature profile.

temperature profile shown in figure 7(a). Independent conventional curing experiments on epoxy 2 found that gelation occurred between 40 °C and 45 °C for two hour treatment; that is a sample exposed to 40 °C remained uncured with a sufficiently low viscosity that all liquid could be removed from a glass slide by gravity, while treatment at 45 °C resulted in a very weak gel. This indicates that epoxy 2 material exposed to temperature greater than 40–45 °C will cure. Examining figure 7(a), the range of distance values where the temperature drops to 40–45 °C matches very well with the observed cured epoxy thickness.

Thus the width of a cured epoxy line is well-predicted by temperature profiles such as figure 7(a). The temperature decay with distance from the irradiated region outwards is dependent upon the magnitude of heat loss in the system, which in this geometry varies with the thickness of the liquid bath, the presence or absence of forced air circulation at the surface, and the composition of the substrate. In general, large losses are associated with steeper temperature profiles and thus, produce samples with narrower lines. For both epoxy systems tested, heat loss was relatively insensitive to these parameters and thus the temperature above ambient due to the photothermal heating reliably dropped to one-half of its maximum value within ~1 mm distance from the intentionally heated zone.

4. Conclusion

We have demonstrated a facile method for incorporating metal nanoparticles into epoxy systems at low concentrations in order to enable *in situ* curing via photothermal heating. Strategies are presented to control the viscosity of the epoxy +AuNP liquid, in particular by pre-curing or slight swelling of the epoxy matrix so that such liquids could be utilized as core fluids in a variety of fibrous geometries or pumped via syringe. By utilizing exchange from water to a solvent miscible with the epoxy matrix, nanoparticles can be uniformly well dispersed. The mechanical properties of the cured epoxy are identical under either heating modality, photothermal or conventional. By utilizing rastering, photothermal curing can be achieved with moderate laser intensities accessible with relatively low power commercial diode lasers. Photothermal heating enables selective curing of an arbitrary shape within a liquid bath of epoxy, leaving the remainder unaltered. The temperature profile across the sample including the drop in temperature from the irradiated region outward is discussed and measured. The breadth of the temperature profile determines the width of the resultant cured epoxy line when curing from a bath and is also a measure of the warming of material away from the irradiated zone during photothermal heating *in situ*. In general, the temperature drops sharply over a ~1 mm distance.

Acknowledgments

This work was supported by the National Science Foundation (CMMI-0829379, CMMI-1069108) and the Faculty Research and Professional Development Fund at North Carolina State University. We would like to thank Dr Keith Weninger (NCSU Physics), the Analytical Services Laboratory (NCSU Textile Engineering, Chemistry, and Science) and the Education and Research Laboratory (NCSU Physics) for use of equipment. This work was performed in part at the Analytical Instrumentation Facility (AIF), which is supported by the State of North Carolina and the National Science Foundation (award number ECCS-1542015). The AIF is a member of the North Carolina Research Triangle Nanotechnology Network (RTNN), a site in the National Nanotechnology Coordinated Infrastructure (NNCI).

References

[1] Harley B A C, Kim H D, Zaman M H, Yannas I V, Lauffenburger D A and Gibson L J 2008 Microarchitecture of three-dimensional scaffolds influences cell migration behavior via junction interactions *Biophys. J.* **95** 4013–24

[2] Oh S H, An D B, Kim T H and Lee J H 2016 Wide-range stiffness gradient PVA/HA hydrogel to investigate stem cell differentiation behavior *Acta Biomater.* **35** 23–31

[3] Owen S C and Shoichet M S 2010 Design of three-dimensional biomimetic scaffolds *J. Biomed. Mater. Res.* A **94A** 1321–31

[4] Wingate K, Bonani W, Tan Y, Bryant S J and Tan W 2012 Compressive elasticity of three-dimensional nanofiber matrix directs mesenchymal stem cell differentiation to vascular cells with endothelial or smooth muscle cell markers *Acta Biomater.* **8** 1440–9

[5] Wu S L, Liu X M, Yeung K W K, Liu C S and Yang X J 2014 Biomimetic porous scaffolds for bone tissue engineering *Mater. Sci. Eng. R-Rep.* **80** 1–36

[6] Martin J Y, Schwartz Z, Hummert T W, Schraub D M, Simpson J, Lankford J, Dean D D, Cochran D L and Boyan B D 1995 Effect of titanium surface-roughness on proliferation, differentiation, and protein-synthesis of human osteoblast-like cells (MG63) *J. Biomed. Mater. Res.* **29** 389–401

[7] Maity S, Kozek K A, Wu W C, Tracy J B, Bochinski J R and Clarke L I 2013 Anisotropic thermal processing of polymer nanocomposites via the photothermal effect of gold nanorods *Part. Part. Syst. Charact.* **30** 193–202

[8] Maity S, Wu W C, Xu C, Tracy J B, Gundogdu K, Bochinski J R and Clarke L I 2014 Spatial temperature mapping within polymer nanocomposites undergoing ultrafast photothermal heating via gold nanorods *Nanoscale* **6** 15236–47

[9] Maity S, Bochinski J R and Clarke L I 2012 Metal nanoparticles acting as light-activated heating elements within composite materials *Adv. Funct. Mater.* **22** 5259–70

[10] Maity S, Downen L N, Bochinski J R and Clarke L I 2011 Embedded metal nanoparticles as localized heat sources: an alternative processing approach for complex polymeric materials *Polymer* **52** 1674–85

[11] Eustis S and El-Sayed M A 2006 Why gold nanoparticles are more precious than pretty gold: noble metal surface plasmon resonance and its enhancement of the radiative and nonradiative properties of nanocrystals of different shapes *Chem. Soc. Rev.* **35** 209–17

[12] Liz-Marzan L M 2006 Tailoring surface plasmons through the morphology and assembly of metal nanoparticles *Langmuir* **22** 32–41

[13] Link S and El-Sayed M A 1999 Spectral properties and relaxation dynamics of surface plasmon electronic oscillations in gold and silver nanodots and nanorods *J. Phys. Chem.* B **103** 8410–26

[14] Tsai M F, Chang S H G, Cheng F Y, Shanmugam V, Cheng Y S, Su C H and Yeh C S 2013 Au nanorod design as light-absorber in the first and second biological near-infrared windows for *in vivo* photothermal therapy *ACS Nano* **7** 5330–42

[15] Huang X H, Jain P K, El-Sayed I H and El-Sayed M A 2008 Plasmonic photothermal therapy (PPTT) using gold nanoparticles *Lasers Med. Sci.* **23** 217–28

[16] Huang X H, Neretina S and El-Sayed M A 2009 Gold nanorods: from synthesis and properties to biological and biomedical applications *Adv. Mater.* **21** 4880–910

[17] Tumbleston J R *et al* 2015 Continuous liquid interface production of 3D objects *Science* **347** 1349–52

[18] Kalele S A, Tiwari N R, Gosavi S W and Kulkarni S K 2007 Plasmon-assisted photonics at the nanoscale *J. Nanophoton.* **1** 20

[19] Jain P K, Lee K S, El-Sayed I H and El-Sayed M A 2006 Calculated absorption and scattering properties of gold nanoparticles of different size, shape, and composition: applications in biological imaging and biomedicine *J. Phys. Chem.* B **110** 7238–48

[20] Murphy C J, Gole A M, Stone J W, Sisco P N, Alkilany A M, Goldsmith E C and Baxter S C 2008 Gold nanoparticles in biology: beyond toxicity to cellular imaging *Acc. Chem. Res.* **41** 1721–30

[21] Berven C A, Clarke L, Mooster J L, Wybourne M N and Hutchison J E 2001 Defect-tolerant single-electron charging at room temperature in metal nanoparticle decorated biopolymers *Adv. Mater.* **13** 109–13

[22] Berven C A, Wybourne M N, Clarke L, Hutchison J E, Brown L O, Mooster J L and Schmidt M E 2000 The use of biopolymer templates to fabricate low-dimensional gold particle structures *Superlatt. Microstruct.* **27** 489–93

[23] Berven C A, Wybourne M N, Clarke L, Longstreth L, Hutchison J E and Mooster J L 2002 Background charge fluctuations and the transport properties of biopolymer-gold nanoparticle complexes *J. Appl. Phys.* **92** 4513–7

[24] Clarke L, Wybourne M N, Brown L O, Hutchison J E, Yan M, Cai S X and Keana J F W 1998 Room-temperature Coulomb-blockade-dominated transport in gold nanocluster structures *Semicond. Sci. Technol.* **13** A111–4

[25] Govorov A O and Richardson H H 2007 Generating heat with metal nanoparticles *Nano Today* **2** 30–8

[26] Lal S, Clare S E and Halas N J 2008 Nanoshell-enabled photothermal cancer therapy: impending clinical impact *Acc. Chem. Res.* **41** 1842–51

[27] Frens G 1973 Controlled nucleation for regulation of particle-size in monodisperse gold suspensions *Nat. Phys. Sci.* **241** 20–2

[28] Haiss W, Thanh N T K, Aveyard J and Fernig D G 2007 Determination of size and concentration of gold nanoparticles from UV–vis spectra *Anal. Chem.* **79** 4215–21

[29] Bohren C F and Huffman D R 2008 *Absorption and Scattering of Light by Small Particles* (New York: Wiley)

[30] Viswanath V, Maity S, Bochinski J R, Clarke L I and Gorga R E 2013 Thermal annealing of polymer nanocomposites via photothermal heating: effects on crystallinity and spherulite morphology *Macromolecules* **46** 8596–607

[31] Abbott D B, Maity S, Burkey M T, Gorga R E, Bochinski J R and Clarke L I 2014 Blending with non-responsive polymers to incorporate nanoparticles into shape-memory materials and enable photothermal heating: the effects of heterogeneous temperature distribution *Macromol. Chem. Phys.* **215** 2345–56

[32] Dell'Erba I E, Hoppe C E and Williams R J J 2010 Synthesis of silver nanoparticles coated with oh-functionalized organic groups: dispersion and covalent bonding in epoxy networks *Langmuir* **26** 2042–9

[33] Qin Z P and Bischof J C 2012 Thermophysical and biological responses of gold nanoparticle laser heating *Chem. Soc. Rev.* **41** 1191–217

[34] Ding T, Valev V K, Salmon A R, Forman C J, Smoukov S K, Scherman O A, Frenkel D and Baumberg J J 2016 Light-induced actuating nanotransducers *Proc. Natl Acad. Sci. USA* **113** 5503–7

[35] Jain P K, Huang X H, El-Sayed I H and El-Sayed M A 2008 Noble metals on the nanoscale: optical and photothermal properties and some applications in imaging, sensing, biology, and medicine *Accounts Chem. Res.* **41** 1578–86